

Free Thiols Regulate the Interactions and Self-Assembly of Thiol-Passivated Metal Nanoparticles

Pan Sun,¹ Linsey M. Nowack,¹ Wei Bu, Mrinal K. Bera, Sean Griesemer, Morgan Reik, Joshua Portner, Stuart A. Rice,* Mark L. Schlossman,* and Binhua Lin*

Cite This: *Nano Lett.* 2021, 21, 1613–1619

Read Online

ACCESS |

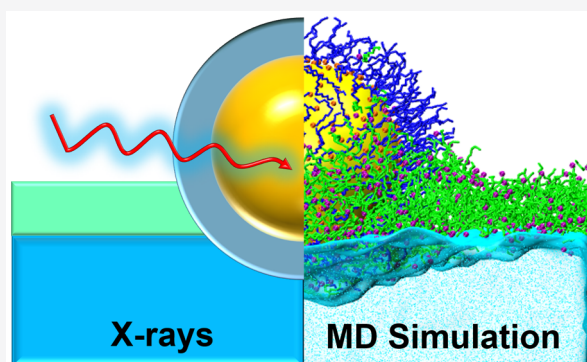
Metrics & More

Article Recommendations

Supporting Information

ABSTRACT: Thiol ligands bound to the metallic core of nanoparticles determine their interactions with the environment and self-assembly. Recent studies suggest that equilibrium between bound and free thiols alters the ligand coverage of the core. Here, X-ray scattering and MD simulations investigate water-supported monolayers of gold-core nanoparticles as a function of the core-ligand coverage that is varied in experiments by adjusting the concentration of total thiols (sum of free and bound thiols). Simulations demonstrate that the presence of free thiols produces a nearly symmetrical coating of ligands on the core. X-ray measurements show that above a critical value of core-ligand coverage the nanoparticle core rises above the water surface, the edge-to-edge distance between neighboring nanoparticles increases, and the nanoparticle coverage of the surface decreases. These results demonstrate the important role of free thiols: they regulate the organization of bound thiols on the core and the interactions of nanoparticles with their surroundings.

KEYWORDS: nanoparticles, ligand symmetry, liquid surface, free thiol



Self-assembly of nanoparticles promises to facilitate the production of liquid surfaces with tunable nanoscale properties.^{1–8} Ligands that coat the surface of the core of a nanoparticle determine its interactions with the liquid surface and, ultimately, nanoparticle self-assembly and surface ordering.^{9–11} Although much effort has gone into designing ligands to produce specific interactions and to direct nanoparticle assembly toward a desired final structure, much less is known about the organization of ligands on the core and how that organization influences interactions and self-assembly.

Molecular dynamics (MD) simulations have explored the local structure of nanoparticle ligands in a variety of environments, including near interfaces.^{12–14} For example, Grest and co-workers demonstrated the asymmetrical ordering of alkanethiol ligands on gold cores situated in the asymmetric environment of a liquid–vapor interface.^{15–17} In this work and in most subsequent MD studies, there are no free thiols in the vicinity of the ligated nanoparticles, either in the nanoparticle suspension or at the interface.⁸ However, recent work has demonstrated that exchange of thiol ligands bound to the core with free thiols in the nanoparticle suspension can alter the core-ligand coverage θ , as the two ensembles of molecules—bound and free—equilibrate.¹⁸ Here, θ is defined as the fraction of the core surface covered by bound ligands as if they were closely packed. Equilibrium between bound and free thiols has been quantified by combining the known

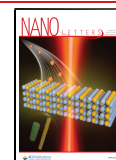
equilibrium adsorption constant with a Langmuir adsorption isotherm to relate the measured concentration of total thiol molecules (sum of bound and free thiols) in a solution of nanoparticles to the core-ligand coverage. A correlation between the availability of free thiols in the nanoparticle suspension and the morphology and mechanical properties of self-assembled nanoparticle monolayers prepared from those suspensions has been observed, but the role of free thiols is unknown.¹⁹

To reveal the role of free thiols on nanoparticle ordering and interactions, we measured the nanoscale structure of monolayers of nanoparticles with different values of core-ligand coverage. Nanoparticles with a particular value of core-ligand coverage, θ , were prepared by equilibrating a chosen mass fraction of total thiols and nanoparticles within a solution that was then spread on the surface of water (see section 2 and Figure S10 in the Supporting Information). As illustrated in Figure 1, several different experimental techniques and complementary MD simulations were used to characterize

Received: October 16, 2020

Revised: January 28, 2021

Published: February 3, 2021



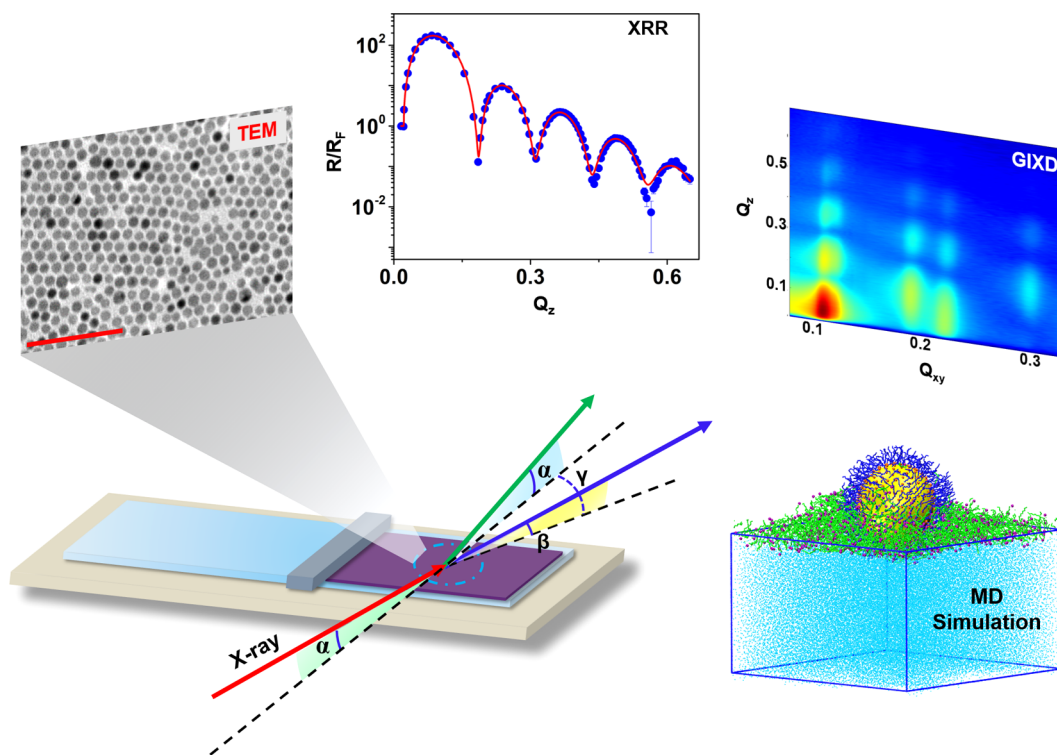


Figure 1. Schematic of experimental geometry for *in situ* X-ray measurements of a monolayer array of nanoparticles supported on the water surface. X-rays shine onto a macroscopically large water surface to reveal the nanoscale ordering of nanoparticles and ligands. X-ray reflectivity (XRR) measures the electron density profile along the interfacial depth of the entire interfacial structure, which includes the effects of both ordered and disordered regions of nanoparticles and free thiols. Analysis of two-dimensional Bragg rods observed by grazing incidence X-ray diffraction (GIXD) characterizes the ordered regions of nanoparticles on the surface. Classical molecular dynamics (MD) simulations of single nanoparticles on the water surface reveal the free and core-ligand conformations, as well as the positioning and influence of the nanoparticle on the water surface. In addition, nanoparticles are separately imaged with transmission electron microscopy (TEM, scale bar 50 nm) to characterize their polydispersity (Figures S9 and S11).

the nanoscale ordering of this nanoparticle system for a range of values of core-ligand coverage. Grazing-incidence X-ray diffraction characterized the hexagonal unit cell of 2D nanoparticle packing, as well as the edge-to-edge distance between neighboring nanoparticles within ordered regions of nanoparticles.¹⁸ Analysis of X-ray reflectivity data with a new model characterized both ordered and disordered regions of the surface to reveal the position of the nanoparticles above the water surface, the thickness of the free thiol film, and the surface coverage of ordered nanoparticle domains in coexistence with disordered thiol film. These quantities are nearly constant over a wide range of core-ligand coverage up to a critical value, beyond which they vary with core-ligand coverage. MD simulations illustrate the surprising result that the core-ligand region becomes symmetric in the presence of free thiols on the water surface. Furthermore, these free thiols wet the periphery of the nanoparticles and form an adjacent surface film with a substantial distribution of thiol headgroups throughout the film thickness. Metrical evaluation of the simulations supports the X-ray analysis, which is consistent with the symmetrization of the ligand coating and the presence of a thinner core-ligand coating in the contact region between neighboring nanoparticles.

These investigations demonstrate that the presence of free thiols has a substantial effect on the ordering of nanoparticles on the water surface. Although the addition of free thiols in these experiments and simulations may at first appear artificial, it is important to remember that in the case of thiolated ligands

on Au-core nanoparticles free thiols are expected to be generally present as a result of equilibration of nanoparticles with their solvent environment. The effort normally applied to remove all free thiols in a nanoparticle solution, a procedure known as “washing” the solution, reduces but does not eliminate free thiols.⁸ In addition, this reduction of free thiols reduces the core-ligand coverage.¹⁸ The effects presented here are expected to be relevant even when free thiols are not replenished after washing.

■ MOLECULAR DYNAMICS (MD) SIMULATIONS

Results from all-atom classical MD simulations of a gold nanoparticle coated by dodecanethiol ligands on the water surface are shown in Figure 2. Simulations were run with different fixed values of core-ligand coverage θ , whose maximal value of 1.0 corresponds to 4.6 ligands/nm². This value was chosen from the known packing of dodecanethiol ligands on flat surfaces that correspond to the flat facets expected for the Au core, although the simulations modeled the core as spherical.^{20,21} Ligands were randomly positioned on a 5 nm diameter spherical core surface and then fixed in place throughout the simulation; refer to the Supporting Information for simulation methods. Two sets of simulations are illustrated in Figure 2: a set with an otherwise bare water surface and a set with a water surface covered by free dodecanethiol molecules—in addition to the ligands fixed to the core—that initially covered the entire water surface with an area per molecule of 25 Å².

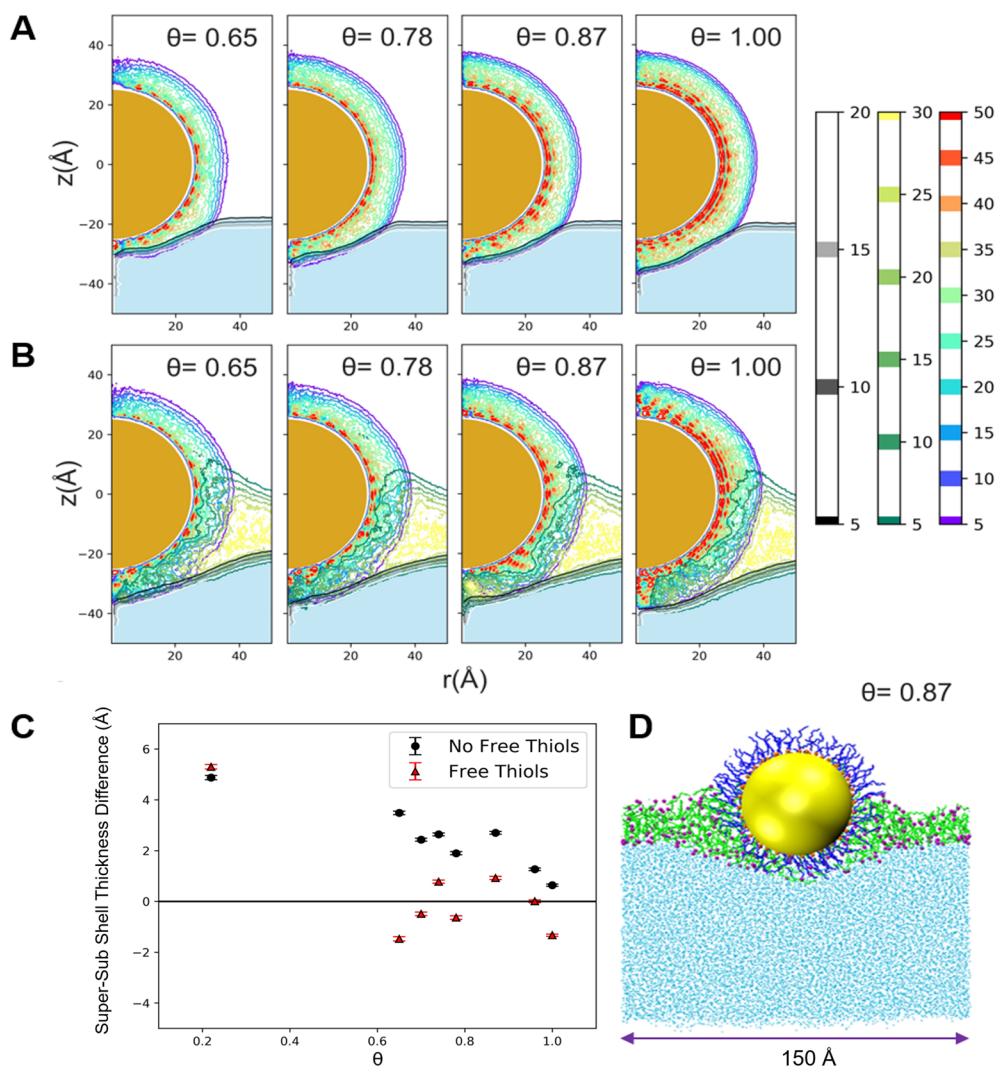


Figure 2. Molecular dynamics (MD) simulations. Contour plots of the spatial distribution of specific atoms for (A) simulations of a nanoparticle on a bare water surface and (B) simulations with additional free thiol molecules on the water surface. Contour plots are spatially averaged over the azimuthal angle in cylindrical coordinates centered on the nanoparticle position and temporally averaged over the last 0.5 ns of the simulation. The center of the Au core is relocated to $z = 0$ Å. Core-ligand coverages, θ , were fixed to the following values: 0.65, 0.78, 0.87, and 1.0 (see Figures S3 and S4 for other values of θ). Colored scales represent density in atoms/nm³: gray scale for oxygen atoms; green scale for carbons in the free thiol layer; rainbow scale for carbons in the thiol ligands bound to the gold core. (C) Differences between the ligand thickness at the bottom (sub) and top (super) of the nanoparticle calculated in the presence and absence of free thiols. Error bars are calculated from the standard error of thickness difference from the average over time. (D) Molecular view for $\theta = 0.87$ that illustrates the distribution of thiol headgroups throughout the dodecanethiol film (see also Figure S5 for other snapshots). Sulfur atoms in free thiols are indicated by purple dots, free thiol chains by green, bound thiol ligands by dark blue and their sulfur atoms by orange, and water oxygen by light blue.

Simulations of a nanoparticle at the bare water surface in Figure 2A illustrate features previously observed:^{8,15} (1) the AuNP is partially submerged (~ 10 Å) within the water slab, (2) the thickness of the ligand coating in contact with water is thinner than elsewhere on the core, and (3) this asymmetry in the ligand coating thickness decreases as the core-ligand coverage increases to 1.0. However, Figure 2B suggests that, for a nanoparticle in the presence of free thiols, asymmetry between the top and bottom of the ligand coating thickness is less pronounced. The difference between the ligand thickness at the bottom and top of the nanoparticle is illustrated in Figure 2C, which shows that in the presence of free thiol the thickness values are nearly the same and the ligand coating is nearly symmetric. In the absence of free thiols, a nearly symmetric coating is achieved only at the highest core-ligand coverage. Different contour coloring in Figure 2B reveals that

the symmetrization of the coating occurs because free thiols mix into the ligand coating in the region of contact between nanoparticle and water. Free thiols also wet the perimeter of the nanoparticle by mixing into the ligand coating further up the nanoparticle, as illustrated in Figure 2B by the rise in free thiol contour and the thickening of the free thiol layer immediately adjacent to the nanoparticle. Both the symmetrization and the wetting may be aided by the unusual molecular ordering within the free thiol film shown in Figure 2D, in which a substantial fraction of the sulfur headgroups are dispersed throughout the film thickness. This is in contrast to the results of MD simulations and X-ray reflectivity from a free monolayer of thiols in the absence of nanoparticles, for which sulfur headgroups are primarily in contact with water (Figures S6, S13, and S14).

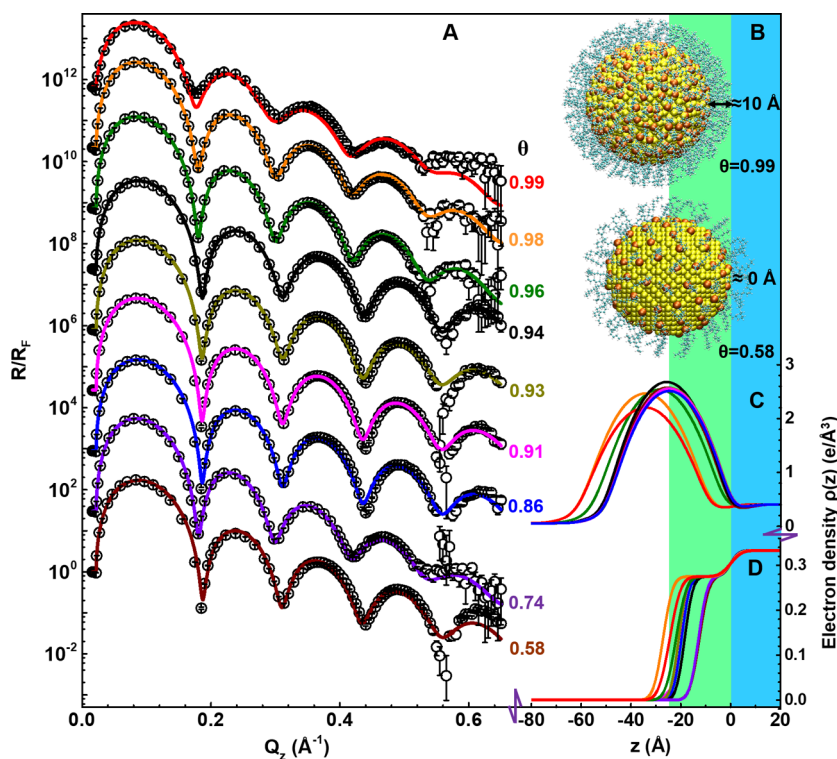


Figure 3. X-ray reflectivity measurements from water surfaces containing a partial monolayer of dodecanethiol ligated Au nanoparticles in coexistence with free dodecanethiol molecules. (A) X-ray reflectivity R (normalized to the Fresnel reflectivity R_F from an idealized water surface) as a function of wave vector transfer, Q_z , normal to the surface. Data points are indicated by the open circles, and solid lines are fits described in the text and the Supporting Information. Each set of data is measured from nanoparticles with a different core-ligand coverage, θ , as indicated in the figure, which is determined by the total-thiol concentration in the spreading solution (section 2 in the Supporting Information). (B) Cartoons of nanoparticles that illustrate the position of nanoparticles above the water surface ($z < 0$, to the left of the green/blue boundary) for the highest and lowest values of measured θ . These cartoons are drawn from the electron density profiles measured by X-ray reflectivity. (C) Electron density profiles of the nanoparticle regions of the surface that illustrate the shift away from the water surface for $\theta > 0.95$. (D) Electron density profiles of the free thiol film regions of the surface that illustrate the gradual increase in thickness of the film. The coordinate z measures distances perpendicular to the surface plane. The color coding of lines in parts C and D is the same as that for the fits in part A.

■ X-RAY MEASUREMENTS

X-ray measurements were performed at 15-ID-C, NSF's ChemMatCARS beamline, at the Advanced Photon Source, Argonne National Laboratory. X-ray reflectivity probes the positioning of nanoparticles and free thiols on the water surface by measuring the electron density profile $\rho(z)$ along the z -axis perpendicular to the surface but averaged over the x - y plane of the surface.²² Figure 3 illustrates nine data sets, each corresponding to a sample of nanoparticles with a different value of core-ligand coverage, θ . The oscillations in the data have a shape characteristic of the parabolic electron density profile that results from nearly spherical gold-core nanoparticles on a surface; the detailed shape of the reflectivity provides information on the arrangement of nanoparticles and free thiols with subnanometer spatial resolution.

The reflectivity data in Figure 3 cannot be fit by a single monolayer of nanoparticles that fills the surface. Instead, coexisting regions of nanoparticles and free thiols must be considered, which is consistent with our observations from TEM shown in Figure S11. The model for the free thiol region is a simple slab, as suggested by simulations, with an electron density fixed at the value from simulations, $0.275 \text{ e}^- \text{ \AA}^{-3}$, but with thickness d as a fitting parameter. The model for the nanoparticle region of the surface is illustrated in Figure 4. Analytic details of the model are provided in the Supporting

Information (see section 3.3 and Figure S15 in the Supporting Information).

Figure 4A illustrates a top view of the hexagonal packing of the nanoparticle region of the monolayer. Grazing-incidence X-ray diffraction (GIXD) from the water surface, as illustrated in Figure 1, was measured from the same samples studied by X-ray reflectivity (see Figure S12 for GIXD analysis). The in-plane Q_{xy} positions of the four Bragg rods shown in Figure 1 determined the hexagonal unit cell parameters (Table S2). The variation in X-ray intensity along the Bragg rod (in the out-of-plane Q_z direction) determined the average core diameter in the hexagonally ordered region of the surface. Combining these two measured values yields the edge-to-edge distance of closest approach, D_{e-e} , between neighboring Au cores shown in Figure 4B and listed in Table S2. Values of D_{e-e} were used in the analysis of X-ray reflectivity data.

The region of closest approach between nanoparticles should contain ligands from both nanoparticles, yet the edge-to-edge distance, D_{e-e} , is usually less than twice the value of ligand thickness, l_c (see Figure 4B), observed in MD simulations. Including this feature of confined ligands significantly improved fits to the X-ray reflectivity data (Figures S17 and S18). Additional features of significance for fitting X-ray reflectivity data included polydispersity of the core sizes and setting the bottom of the ligand shell of all nanoparticles to be at the same interfacial depth (as shown in Figure 4B). The

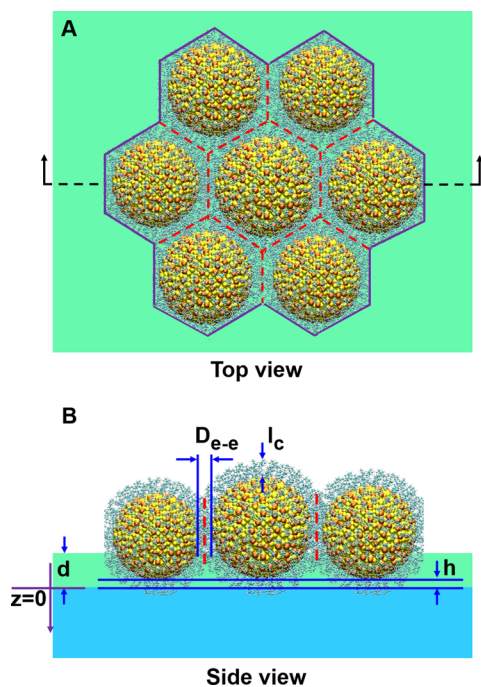


Figure 4. Real space model used to construct the electron density profile to fit X-ray reflectivity measurements. (A) Top view showing hexagonally packed nanoparticles. (B) Side cross-sectional view obtained by cutting along the dashed line in part A. The green slab represents the free thiol film of thickness d , and blue represents water. The nanoparticle height h is the distance from the bottom of the Au core to the water surface, where $h < 0$ is shown. The distance D_{e-e} is the edge-to-edge distance of closest approach between neighboring Au cores, and l_c is the ligand thickness away from the region of closest approach.

latter positioning of the nanoparticles is consistent with nanoparticle–environment interactions dominated by the outermost portion of the ligand shell. Relaxing these features by using, for example, (a) monodisperse nanoparticles with height fluctuation or (b) use of a constant ligand thickness all the way around the core yielded significantly worse fits to the reflectivity data (see section 3.3.3 in the Supporting Information for detailed error analyses). Note, however, that the top–bottom symmetry of the ligand coating was maintained in fitting X-ray reflectivity data, as suggested by MD simulations. Fitting with a model containing a variable asymmetry of the ligand coating yielded fits of similar quality as those that assumed symmetric core–ligands, indicating that X-ray reflectivity is not sensitive to the asymmetry in this system.

As illustrated in Figure 5A, the bottom of the Au core was measured by X-ray reflectivity to be at the height of the water surface for values of core–ligand coverage $\theta < 0.95$ but rises nearly a nanometer above the water surface as θ approaches 1. Similarly, Figure 5B shows that the edge-to-edge distance D_{e-e} is relatively constant at 17 Å until the critical value of $\theta = 0.95$, above which it rises to 25 Å, which is essentially twice the ligand thickness $l_c = 12.5$ Å observed in the MD simulations. The denser ligands on the core are either resistant to being confined in the region of closest approach between Au cores or resist mixing of core–ligands from neighboring nanoparticles. In a similar way, denser core–ligands may resist mixing with free thiols on the water surface, leading to the increase in height shown in Figure 5A.

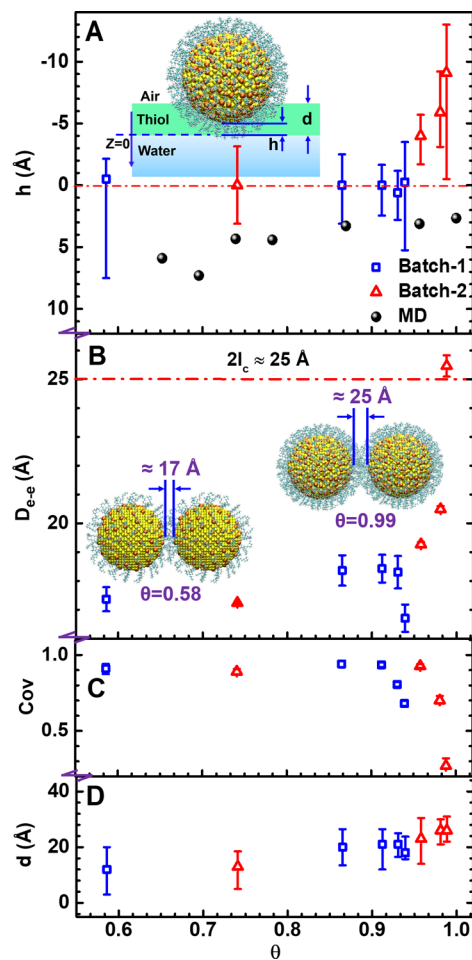


Figure 5. Results from fitting X-ray reflectivity measurements in Figure 3 and GIXD measurements in Figure S12 that quantified the nanoparticle/thiol ordering at the water surface as a function of core–ligand coverage, θ . Results are shown from two sources of nanoparticles with diameters that differed by ~ 1.4 Å (batch 1 and 2 nanoparticles have core diameters of 51.6 and 53 Å, respectively). Batch 1 results are shown by blue squares for $\theta = 0.58, 0.86, 0.91, 0.93,$ and 0.94 , and batch 2 results are shown by red triangles for $\theta = 0.74, 0.96, 0.98,$ and 0.99 . (A) Nanoparticle height h , where $h < 0$ is shown by the configuration in the inset. Positive h corresponds to penetration of the Au core below the water surface. (B) Edge-to-edge distance of closest approach D_{e-e} between neighboring Au cores. (C) Fractional coverage of nanoparticles on the water surface. The rest of the surface is covered by a thin film of free thiols. (D) Thickness d of the thin film of free thiols.

Also shown in Figure 5A, MD simulations do not exhibit the rise in height h for $\theta > 0.95$. This may be due to modeling the Au core as a sphere instead of a polyhedral Au crystal with flat facets. Core–ligands on a spherical or curved surface are more loosely packed,²³ and free thiols can mix into the region of bound ligands even at the close-packed value of 4.6 ligands/nm² for which free thiols would be excluded from mixing with close-packed ligands bound to a flat surface. In addition, an offset of roughly 3–5 Å appears to place the gold core deeper into the water in the MD simulations. This is likely an artifact of the single nanoparticle simulations. Nevertheless, a two-nanoparticle simulation (see Figure S8) does not appear to resolve this issue. Future work may be able to address this issue with a configuration of three nanoparticles in a triangle, as this

is the smallest version of the symmetry and packing in the monolayer.

Figure 5C quantifies the fraction of the water surface covered by nanoparticles; the remainder of the surface is covered by free thiol film. The nanoparticle coverage drops rapidly at higher values of ligand-core coverage, which corresponds to larger numbers of free thiol molecules on the water surface. The critical value for this change appears to be different for the two different batches of nanoparticles studied. The diameters of these batches differed by ~ 1.4 Å. Although it is possible that size effects play a role in this observation, the mechanism is not understood at present.

As shown in Figure 5D, the thickness d of the free thiol film varies from 12 to 26 Å with increasing θ , as previously illustrated by the electron density profiles in Figure 3D. The all-trans length of dodecanethiol is roughly 17.7 Å, so that this film thickness corresponds to a disordered film of roughly one to two layers of molecules. As shown in Figures 2D and S6, the disorder within the simulated film, which locates thiol headgroups throughout the film, enables a continuous range of thickness values.

SUMMARY

Our MD simulations and X-ray surface scattering results demonstrate the consequences of equilibrium between thiol ligands on a nanoparticle gold core and free thiols in the environment, for the particular case of nanoparticles self-assembled on the surface of water in the presence of varying amounts of free thiols on that surface. This equilibration determines the coverage of the core by bound ligands. MD simulations demonstrate that intermixing or interdigitation of free thiols with the thiol ligands bound to the gold core produces a nearly symmetric ligand coating of the core (Figure 2B) in contrast to the asymmetric coating observed in the absence of free thiols except at the highest value of core-ligand coverage (Figure 2A). X-ray measurements suggest that above a critical value of core-ligand coverage ($\theta = 0.95$) the ligand coating becomes resistant to the intermixing or interdigitation of free thiols. Evidence for this includes the measured rise in nanoparticles above the water surface for $\theta > 0.95$, as well as the increase in edge-to-edge spacing between the Au cores. The edge-to-edge spacing varies from values well below twice the thickness of the ligand coating for $\theta < 0.95$ to twice the thickness for $\theta = 0.99$, corresponding to having a robust layer of core-ligands on each nanoparticle that excludes the interdigitation of ligands from neighboring nanoparticles.

It is difficult to avoid the presence of free thiols in the preparation of nanoparticles with Au cores coated by thiol ligands because of the relatively weak thiol-gold bond. As a result, thiol ligands on the gold core are in equilibrium with free thiols in the environment. As we have demonstrated for nanoparticle assemblies supported on the water surface, equilibration of thiol ligands with free thiols will alter the core-ligand coverage and, thereby, influence the ordering and assembly of nanoparticle arrays. The presence of free thiols is likely also responsible for elastic properties of 2D nanoparticle assemblies on the water surface previously observed under conditions in which the concentration of free thiols was varied. In particular, monolayers of extensively washed AuNPs ($\theta \sim 0.6$ – 0.7) undergo monolayer to wrinkle transitions under lateral compression, whereas monolayers of AuNPs with $\theta > 0.8$ will undergo monolayer to buckling transitions under lateral compression.^{19,24} These nanoscale effects of the free

thiols may be explained by our model of AuNP assembly on the water surface in the presence of free thiols (Figure S15). At lower θ , where the interparticle spacing is smaller, the interactions of bound ligands of neighboring AuNPs may be enhanced so that the nanoparticles form a 2D elastic sheet which can wrinkle under compression.^{25,26} As θ is increased, the spacing between AuNPs increases, resulting in decreased interactions of bound ligands between neighboring AuNPs. In addition, free thiols may fill the space between AuNPs, thereby further reducing the monolayer bending rigidity to an extent that monolayers buckle instead of wrinkle. More generally, we anticipate that the effects that we have observed will be present for thiol ligands of different chain length, which should also equilibrate with free thiols and alter the core-ligand coverage. Understanding the mechanism of free and bound thiol equilibration, as well as its role in self-assembly, may have a substantial impact on the preparation of nanoparticle assemblies and their performance in a range of applications.

ASSOCIATED CONTENT

Supporting Information

The Supporting Information is available free of charge at <https://pubs.acs.org/doi/10.1021/acs.nanolett.0c04147>.

Materials, experimental methods and analysis, and MD simulations (PDF)

AUTHOR INFORMATION

Corresponding Authors

Stuart A. Rice – James Franck Institute and Department of Chemistry, University of Chicago, Chicago, Illinois 60637, United States; Email: sarice@uchicago.edu

Mark L. Schlossman – Department of Physics, University of Illinois at Chicago, Chicago, Illinois 60607, United States; Email: schloss@uic.edu

Binhua Lin – NSF's ChemMatCARS, University of Chicago, Chicago, Illinois 60637, United States; James Franck Institute, University of Chicago, Chicago, Illinois 60637, United States; orcid.org/0000-0001-5932-4905; Email: lin@cars.uchicago.edu

Authors

Pan Sun – NSF's ChemMatCARS, University of Chicago, Chicago, Illinois 60637, United States; orcid.org/0000-0002-6128-8656

Linsey M. Nowack – James Franck Institute, University of Chicago, Chicago, Illinois 60637, United States

Wei Bu – NSF's ChemMatCARS, University of Chicago, Chicago, Illinois 60637, United States; orcid.org/0000-0002-9996-3733

Mrinal K. Bera – NSF's ChemMatCARS, University of Chicago, Chicago, Illinois 60637, United States

Sean Griesemer – James Franck Institute, University of Chicago, Chicago, Illinois 60637, United States

Morgan Reik – James Franck Institute, University of Chicago, Chicago, Illinois 60637, United States

Joshua Portner – James Franck Institute, University of Chicago, Chicago, Illinois 60637, United States

Complete contact information is available at: <https://pubs.acs.org/doi/10.1021/acs.nanolett.0c04147>

Author Contributions

[†]P.S., L.M.N.: These authors contributed equally.

Notes

The authors declare no competing financial interest.

■ ACKNOWLEDGMENTS

This research is supported by NSF's ChemMatCARS. NSF's ChemMatCARS Sector 15 is funded by the Divisions of Chemistry (CHE) and Materials Research (DMR), National Science Foundation, under grant number NSF/CHE-1834750. We also acknowledge support from the University of Chicago MRSEC NSF/DMR-1420709 for BL and SAR and NSF/DMR-2011854 for JP. Use of the Advanced Photon Source, an Office of Science User Facility operated for the U.S. Department of Energy (DOE) Office of Science by Argonne National Laboratory, was supported by the U.S. DOE under Contract No. DE-AC02-06CH11357.

■ REFERENCES

- (1) Garbin, V.; Crocker, J. C.; Stebe, K. J. Nanoparticles at Fluid Interfaces: Exploiting Capping Ligands to Control Adsorption, Stability and Dynamics. *J. Colloid Interface Sci.* **2012**, *387* (1), 1–11.
- (2) Tang, T. Y.; Zhou, Y.; Arya, G. Interfacial Assembly of Tunable Anisotropic Nanoparticle Architectures. *ACS Nano* **2019**, *13* (4), 4111–4123.
- (3) Yucknovsky, A.; Mondal, S.; Burnstine-Townley, A.; Foqara, M.; Amdursky, N. Use of Photoacids and Photobases To Control Dynamic Self-Assembly of Gold Nanoparticles in Aqueous and Nonaqueous Solutions. *Nano Lett.* **2019**, *19* (6), 3804–3810.
- (4) Bera, M. K.; Chan, H.; Moyano, D. F.; Yu, H.; Tatur, S.; Amoanu, D.; Bu, W.; Rotello, V. M.; Meron, M.; Kral, P.; Lin, B. H.; Schlossman, M. L. Interfacial Localization and Voltage-Tunable Arrays of Charged Nanoparticles. *Nano Lett.* **2014**, *14* (12), 6816–6822.
- (5) Kosif, I.; Kratz, K.; You, S. S.; Bera, M. K.; Kim, K.; Leahy, B.; Emrick, T.; Lee, K. Y. C.; Lin, B. H. Robust Gold Nanoparticle Sheets by Ligand Cross-Linking at the Air-Water Interface. *ACS Nano* **2017**, *11* (2), 1292–1300.
- (6) Wang, L. M.; Quan, P. Y.; Chen, S. H.; Bu, W.; Li, Y. F.; Wu, X. C.; Wu, J. G.; Zhang, L. L.; Zhao, Y. L.; Jiang, X. M.; Lin, B. H.; Zhou, R. H.; Chen, C. Y. Stability of Ligands on Nanoparticles Regulating the Integrity of Biological Membranes at the Nano-Lipid Interface. *ACS Nano* **2019**, *13* (8), 8680–8693.
- (7) Barry, E.; McBride, S. P.; Jaeger, H. M.; Lin, X. M. Ion Transport Controlled By Nanoparticle-Functionalized Membranes. *Nat. Commun.* **2014**, *5*, 5847.
- (8) Jiang, Z.; He, J.; Deshmukh, S. A.; Kanjanaboos, P.; Kamath, G.; Wang, Y.; Sankaranarayanan, S. K.; Wang, J.; Jaeger, H. M.; Lin, X. M. Subnanometre Ligand-shell Asymmetry Leads to Janus-like Nanoparticle Membranes. *Nat. Mater.* **2015**, *14* (9), 912–917.
- (9) Ling, D.; Hackett, M. J.; Hyeon, T. Surface Ligands in Synthesis, Modification, Assembly and Biomedical Applications of Nanoparticles. *Nano Today* **2014**, *9*, 457–477.
- (10) Heuer-Jungemann, A.; Feliu, N.; Bakaimi, I.; Hamaly, M.; Alkilany, A.; Chakraborty, I.; Masood, A.; Casula, M. F.; Kostopoulou, A.; Oh, E.; Susumu, K.; Stewart, M. H.; Medintz, I. L.; Stratakis, E.; Parak, W. J.; Kanaras, A. G. The Role of Ligands in the Chemical Synthesis and Applications of Inorganic Nanoparticles. *Chem. Rev.* **2019**, *119* (8), 4819–4880.
- (11) Kim, Y.; Macfarlane, R. J.; Jones, M. R.; Mirkin, C. A. Transmutable Nanoparticles With Reconfigurable Surface Ligands. *Science* **2016**, *351* (6273), 579–582.
- (12) Hu, Y.; Wu, B.; Xu, Z.; Yang, Z.; Yang, X. Solvation Structure and Dynamics for Passivated Au Nanoparticle in Supercritical CO₂: A Molecular Dynamic Simulation. *J. Colloid Interface Sci.* **2011**, *353* (1), 22–29.
- (13) Lin, J. Q.; Zheng, Y. G.; Zhang, H. W.; Chen, Z. A Simulation Study on Nanoscale Holes Generated by Gold Nanoparticles on Negative Lipid Bilayers. *Langmuir* **2011**, *27* (13), 8323–8332.
- (14) Salorinne, K.; Malola, S.; Wong, O. A.; Rithner, C. D.; Chen, X.; Ackerson, C. J.; Hakkinen, H. Conformation and Dynamics of the Ligand Shell of a Water-Soluble Au₁₀₂ Nanoparticle. *Nat. Commun.* **2016**, *7*, 10401.
- (15) Lane, J. M.; Grest, G. S. Spontaneous Asymmetry of Coated Spherical Nanoparticles in Solution and at Liquid-Vapor Interfaces. *Phys. Rev. Lett.* **2010**, *104* (23), 235501.
- (16) Lane, J. M.; Grest, G. S. Assembly of Responsive-Shape Coated Nanoparticles at Water Surfaces. *Nanoscale* **2014**, *6* (10), 5132–5137.
- (17) Salerno, K. M.; Bolintineanu, D. S.; Lane, J. M. D.; Grest, G. S. Ligand Structure and Mechanical Properties of Single-Nanoparticle-Thick Membranes. *Phys. Rev. E* **2015**, *91* (6), 062403.
- (18) Reik, M.; Calabro, M.; Griesemer, S.; Barry, E.; Bu, W.; Lin, B.; Rice, S. A. The Influence of Fractional Surface Coverage on the Core-Core Separation in Ordered Monolayers of Thiol-Ligated Au Nanoparticles. *Soft Matter* **2019**, *15* (43), 8800–8807.
- (19) Griesemer, S. D.; You, S. S.; Kanjanaboos, P.; Calabro, M.; Jaeger, H. M.; Rice, S. A.; Lin, B. H. The Role of Ligands in the Mechanical Properties of Langmuir Nanoparticle Films. *Soft Matter* **2017**, *13* (17), 3125–3133.
- (20) Pensa, E.; Cortes, E.; Corthey, G.; Carro, P.; Vericat, C.; Fonticelli, M. H.; Benitez, G.; Rubert, A. A.; Salvarezza, R. C. The Chemistry of the Sulfur-Gold Interface: In Search of a Unified Model. *Acc. Chem. Res.* **2012**, *45* (8), 1183–1192.
- (21) Schreiber, F. Structure and Growth of Self-Assembling Monolayers. *Prog. Surf. Sci.* **2000**, *65* (5–8), 151–256.
- (22) Pershan, P. S.; Schlossman, M. L. *Liquid Surfaces and Interfaces: Synchrotron X-ray Methods*; Cambridge University Press: Cambridge, U.K., 2012.
- (23) Salerno, K. M.; Bolintineanu, D. S.; Lane, J. M.; Grest, G. S. High strength, molecularly thin nanoparticle membranes. *Phys. Rev. Lett.* **2014**, *113* (25), 258301.
- (24) Dai, Y.; Lin, B.; Meron, M.; Kim, K.; Leahy, B.; Witten, T. A.; Shpyrko, O. G. Synchrotron X-ray Studies of Rapidly Evolving Morphology of Self-Assembled Nanoparticle Films under Lateral Compression. *Langmuir* **2013**, *29* (46), 14050–14056.
- (25) Leahy, B. D.; Pociavsek, L.; Meron, M.; Lam, K. L.; Salas, D.; Viccaro, P. J.; Lee, K. Y.; Lin, B. Geometric Stability and Elastic Response of A Supported Nanoparticle Film. *Phys. Rev. Lett.* **2010**, *105* (5), 058301.
- (26) Pociavsek, L.; Dellsy, R.; Kern, A.; Johnson, S.; Lin, B.; Lee, K. Y.; Cerda, E. Stress and Fold Localization in Thin Elastic Membranes. *Science* **2008**, *320* (5878), 912–916.